Published in final edited form as:
Cancer Res. 2014 April 1; 74(7): 1913–1923. doi:10.1158/0008-5472.CAN-13-3001.

Apoptosis imaging for monitoring DR5 antibody accumulation and pharmacodynamics in brain tumors non-invasively

Thomas G. Weber[1], **Franz Osl**[1], **Anja Renner**[1], **Thomas Pöschinger**[1], **Stefanie Galbán**[2], **Alnawaz Rehemtulla**[2], and **Werner Scheuer**[1]

[1]Discovery Oncology, Pharmaceutical Research and Early Development (pRED), Roche Diagnostics GmbH, Penzberg, Germany

[2]Department of Radiation Oncology & Center for Molecular Imaging, University of Michigan, Ann Arbor, MI, USA

Abstract

High grade gliomas often possess an impaired blood-brain barrier (BBB) which allows delivery of large molecules to brain tumors. However, achieving optimal drug concentrations in brain tumors remains a significant hurdle for treating patients successfully. Thus, detailed investigations of drug activities in gliomas are needed. To investigate BBB penetration, pharmacodynamics and tumor retention kinetics, we studied an agonistic DR5 antibody in a brain tumor xenograft model to investigate a non-invasive imaging method for longitudinal monitoring of apoptosis induction by this antibody. Brain tumors were induced by intracranial (i.c.) implantation of a luciferase-expressing tumor cell line as a reporter. To quantify accumulation of anti-DR5 in brain tumors, we generated a dose response curve for apoptosis induction after i.c. delivery of fluorescence-labeled anti-DR5 at different dosages. Assuming 100% drug delivery after i.c. application, the amount of accumulated antibody after i.v. application was calculated relative to its apoptosis induction. We found that up to 0.20–0.97% of antibody delivered i.v. reached the brain tumor, but that apoptosis induction declined quickly within 24 hours. These results were confirmed by 3D fluorescence microscopy of antibody accumulation in explanted brains. Nonetheless, significant antitumor efficacy was documented after anti-DR5 delivery. We further demonstrated that antibody crossing the BBB was facilitated its impairment in brain tumors. These imaging methods enable the quantification of antibody accumulation and pharmacodynamics in brain tumors, offering a holistic approach for assessment of CNS targeting drugs.

Keywords

blood-brain barrier; brain tumor; Death Receptor 5 antibody; apoptosis imaging; quantification

Corresponding Author: Thomas Weber, Dipl Molmed, Pharmaceutical Research and Early Development, Discovery Oncology, Roche Diagnostics GmbH, Nonnenwald 2, 82377 Penzberg, Germany. thomas.weber.tw7@roche.com. Phone: +49 (0)8856 60 5118. Fax: +49 (0)8856 60 4612.

Conflicts of interest: Thomas G. Weber, Franz Osl, Anja Renner, Thomas Pöschinger and Werner Scheuer are employees of Roche Diagnostics GmbH. Stefanie Galbán and Alnawaz Rehemtulla have no conflicts of interest.

Introduction

A significant obstacle in the treatment of brain disorders is caused by the restricted diffusion of potential therapeutics through the intact BBB. The BBB is built up by tight junctions that connect brain capillary endothelial cells and foot processes of astrocytes which wrap around the brain vessels to further diminish fenestration and permeability (1). Many approaches such as osmotic BBB disruption, intracerebral microinfusion or brain shuttle systems have been reported to increase delivery of therapeutics into the brain (1–5).

Only some anti-cancer compounds such as temozolomide are known to pass the intact BBB in reasonable amounts (6–8) but, so far, the standard-of-care treatment temozolomide plus radiotherapy only leads to modest clinical efficacy and median survival times of 14.2 months after diagnosis with glioblastoma multiforme (GBM) (9). Therapeutic antibodies have shown promising anti-tumor efficacies on malignant brain tumor cells (10–12) but they could not pass an intact BBB to deploy clinical efficacy (13–15). High grade gliomas, however, are known to diversely compromise the BBB most likely in the hypoxic core region of the tumor and neovasculature in brain tumors might not display the same integrity as the BBB in healthy brain tissue (16–18). Dependent on the grade of BBB impairment by brain tumors, it is expected that 0.1% (intact BBB) to 2.0% (disrupted BBB) of systemically applied antibody could reach the brain tumor (1, 19).

In the clinical situation, these calculations are based on the comparison of antibody concentrations in the cerebral spinal fluid (CSF) and in the circulation after systemic application of the antibody. Alternatively, antibody kinetics in brain tumors can be determined by positron emission tomography using a three-compartment model (20). Holdhoff et al determined concentrations of the tyrosine kinase inhibitor imatinib in intraoperatively obtained brain tumor samples by liquid chromatography and mass spectrometry (21). To determine BBB crossing of antibodies in preclinical orthotoptic xenografts, radio- or fluorescence-labeled antibodies are applied, but quantification of signal intensities of successfully delivered antibody can only be examined in dissected brains fractionated into brain capillaries and brain parenchyma. (22–24). Intravital fluorescence videomicroscopy of exposed brain tumors through a cranial window can be used to investigate vessel maturation, blood flow and distribution of fluorescence-labeled molecules in real time (25, 26).

A detailed investigation of pharmacodynamics and kinetics of anticancer compounds in brain tumors besides efficacy and survival studies, however, has not been reported yet. Therefore, we applied non-invasive apoptosis imaging as a pharmacodynamic read-out after treatment with an anti-DR5 antibody. This bioluminescence-based apoptosis imaging relies on the complementation of split-luciferase components C-Luc and N-Luc to a functional luciferase enzyme after Caspase-3/7-dependent cleavage of the stably transfected apoptosis reporter construct C-Luc-DEVD-N-Luc in tumor cells (Fig. 1) (27, 28). Consequently, the conversion of external added substrate luciferin into oxyluciferin and light emission is proportional to Caspase-3/7 activation and apoptosis induction by anti-DR5.

We have recently shown that anti-DR5 leads to tremendous apoptosis induction in subcutaneous GBM tumors some hours after application (28). However, the more clinical relevant model is the orthotopic implantation of tumor cells to consider the specific brain microenvironment and the influence of the diversely impaired BBB. By intracranial inoculation of these apoptosis reporter GBM cells, the apoptosis reporter is only activated when anti-DR5 crosses the BBB, reaches the tumor cells and induces apoptosis via Caspase-8 and Caspase-3/7 (Fig. 1). The quantification of apoptosis induction could therefore indicate the amount of anti-DR5 which has reached the brain tumor. Moreover, the pharmacodynamics of anti-DR5 in brain tumors can be investigated over time indicating the amount of antibody which has been retained in the tumor.

Compounds targeting the apoptosis pathways and inducing apoptosis via death receptors 4 and 5 have previously shown promising anti-tumor efficacies in preclinical brain tumor models in combination with radiotherapy and chemotherapy (29–31). However, these investigations only relied on survival studies. Here, we quantified pharmacodynamics and the amount of anti-DR5 which crosses the impaired BBB by apoptosis imaging and determined if these amounts are sufficient to deploy anti-tumor efficacy. Moreover, we highlighted the impact of BBB impairment by brain tumors on facilitated antibody penetration into brain tissue.

Materials and Methods

Reagents and anti-DR5 generation

Anti-DR5 antibody, a fully human agonistic antibody to Death Receptor 5, was cloned based on the antibody sequences described in the patent application US 2007/0031414 A1 (32). The variable genes of anti-DR5 were fused in frame with human IgG1 constant lambda and constant heavy chain in standard mammalian expression vectors. Lectin from Bandeiraea simplicifolia (BS-I) was purchased from Sigma Aldrich (St. Louis, MO). Control antibody human IgG (Normal) was purchased from Invitrogen (Camarillo, CA). The antibodies and lectin were labeled in-house with Cy5, Alexa Fluor 647 (A647), or Alexa Fluor 750 (A750) by mono-reactive N-hydroxysuccinimide ester for specific labeling of amine residues according to the manufacturer’s instructions (Invitrogen, Hamburg, Germany).

Cell lines and culture

D54-Caspase-3/7 GloSensor cells (obtained from the Center for Molecular Imaging, Ann Arbor, MI on February 10th 2011) were last tested negative on pathogens by molecular diagnostics infectious disease PCR (Charles River, Wilmington, MA) on October 24th 2012 and were authenticated one week prior to implantation by morphologic and growth curve analysis. The cells were cultured in RPMI1640 medium supplemented with 2 mM glutamine, 10% FCS (all PAN Biotech GmbH, Aidenbach, Germany), and 200 μg/ml G-418 (Roche Diagnostics GmbH, Mannheim, Germany).

Intracranial implantation

Female severe combined immunodeficient hairless outbred (SHO) mice (weight 20 to 27 g) were obtained from Charles River (Sulzfeld, Germany) and were 7 to 9 weeks of age at

initiation of experiments. Mice were anesthetized with i.p. injection of 100 mg/kg ketamine (WDT, Garbsen, Germany) and 10 mg/kg xylazine (Rompun®, Bayer Vital GmbH, Leverkusen, Germany). Scalp was disinfected and removed over the whole right hemisphere of the brain to expose the cranium. The periosteum was removed by a bone scraper. Next, a 0.7 mm burr hole in diameter was drilled 2 mm right of midline and 0.5 mm posterior to bregma with a dental drill. Mice were then placed in a small-animal stereotactic frame (David Kopf Instruments, Tujunga, CA) to allow proper cell inoculation. A 25 µl 22-gauge needle (Hamilton, Höchst, Germany) filled with D54-Caspase-3/7 GloSenor cell suspension (8×10^7 cells per ml) was adjusted in a 60 degree ankle over the burr hole and penetrated 3 mm into the brain tissue. Three µl of the cell suspension (240,000 cells) was slowly injected into the brain. After injection, needle was slowly withdrawn and hole was sealed with Cyano veneer tissue glue (Hager Werken, Duisburg, Germany). All animal studies were approved by the local government (file number 55.2-1-54-2532.2-42-11, Government of Upper Bavaria).

Bioluminescence imaging, randomization and signal analysis

Mice were injected with 150 mg/kg D-luciferin i.p. (Biosynth AG, Staad, Switzerland). Twelve minutes after luciferin application, mice were anesthetized with 2% isofluran and placed in an IVIS Spectrum (Perkin Elmer, Hopkinton, MA) in prone position and measured. Bioluminescent signals were read out as average radiance [p/sec/cm3/sr] in a circular region of interest (ROI) over the cranium with Living Image software (Perkin Elmer, Hopkinton, MA). Every ROI signal was divided by the related ROI signal measured for randomization to get fold induction. Seven days after cell implantation, mice were randomized in treatment groups of 3 to 5 mice each according to their basal bioluminescent signals.

Intravenous and intracranial application of antibody

One day after randomization, anti-DR5-Cy5 was systemically given via the tail vein. To determine a dosage response curve, Cy5-labeled anti-DR5 antibody was injected intracranially at different dosages into the brain. Therefore, mice were anesthetized with 100 mg/kg Ketamin and 10 mg/kg Xylazin i.p., sealing tissue glue was lifted and mouse was fixed in the stereotactic frame. To ensure antibody injection in close proximity to the brain tumor, the same stereotactic coordinates were used as for cell implantation. After slow withdrawal of the syringe, the hole was sealed with tissue glue again. Antibodies were given once for delivery study and thrice for efficacy study. For delivery study, bioluminescent signal of mice was measured twice (4 and 8 hours after treatment) and the higher signal was considered for calculations of delivered amount.

Necropsy

Mice were sacrificed 8 hours after (last) drug application. Ten minutes before sacrifice, mice were injected i.v. with 100 µl of a 1 mg/ml lectin-A750 solution to allow visualization of blood vessels *ex vivo*. Mice were sacrificed by cervical dislocation. Brain was explanted and transferred to 10% formalin solution.

3D-imaging of solvent-cleared organs (3DISCO) and determination of TGI and antibody accumulation

3DISCO was performed as previously described (33). Briefly, brain tissues or s.c. tumors were dehydrated in tetrahydrofuran (THF, Sigma Aldrich, St. Louis, MO) dilution series (50%, 70%, 80%, 3× 100% for 12 hours each) and cleared in dibenzyl ether (DBE, Sigma Aldrich, St. Louis, MO) for 2 days. The cleared samples were placed in a light sheet ultramicroscope (LaVision Biotec, Bielefeld, Germany) equipped with a MVX10 Fluorescence MacroZoom, a 2× Mv PLAPO 2VC objective lens (both Olympus, Tokyo, Japan) and an Imager 3QE camera (LaVision Biotec). The samples were scanned with a standard magnification of 0.63× in 5.1 μm thick virtual sections with Cy5 (antibody signal) and A750 (lectin vessel staining) filter settings. Tiff raw data were converted to dicom files which were processed and 3D-reconstructed by OsiriX software (Pixmeo, Geneva, Switzerland). A 3-dimensional brain tumor ROI was defined according to the dimensions of chaotic vessel structures seen by lectin-A750 staining. The determined 3D-ROI was imported to 3D-reconstructed antibody-Cy5 data files to read out brain tumor volumes and mean antibody fluorescent signals within the tumors (fluorescent signal intensities of circulating antibody in blood vessels were subtracted). Representative 3DISCO images in 2D were depicted with maximal intensity projection (MIP) of 10 consecutive virtual sections.

Subcutaneous xenograft model

Female SHO mice (weight 20 to 27 g) were obtained from Charles River (Sulzfeld, Germany) and were 7 to 9 weeks of age at initiation of experiments. Four million D54-Caspase 3/7 GloSensor cells in 100 μl PBS were inoculated in the right flank of each mouse under 2% isofluran anesthesia. After 7 days, the animals were randomized in therapy groups (5 mice per group) according to their basal bioluminescent signal and their tumor volume. All animal studies were approved by the local government (file number 55.2-1-54-2532.2-26-09, Government of Upper Bavaria).

Determination of antibody penetration from vessels to tissue

For antibody penetration studies, 4 mice each with detectable brain tumors, without brain tumors and with s.c. tumors were treated with 5 mg/kg human IgG-A750 for 8 hours and 100 μg lectin-A647 was applied 10 minutes before sacrifice. Necropsy and 3DISCO was conducted as described above. The distinct fluorescent signal intensities of IgG-A750 at different distances from nearest lectin-A647 stained blood vessels for healthy brain, brain tumor, and s.c. tumor tissue were determined as recently described by Dobosz et al with an in-house developed quantification software (34) and the area under these curves (AUC) were calculated.

Immunhistological staining

Cleared samples were removed from DBE solution, washed once with xylole, incubated in paraffin at 60°C for 1 hour (4 times), and blocked in paraffin. Cut paraffin sections (2.5 μm) were stained with haematoxylin and eosin (H&E) and cleaved Caspase-3 in consecutive sections. Cleaved Caspase-3 (D175) rabbit antibody (1:300, Cell Signaling, Danvers, MA)

was incubated for 60 minutes after deparaffinization, steam-heating at 96 °C for 15 minutes and protein blocking. Alexa Fluor 555 goat anti-rabbit IgG (1:300, Invitrogen, Darmstadt, Germany) as secondary antibody was incubated for 30 minutes. Sections were coverslipped with Fluoro-Gel II with DAPI (Electron Microscopy Sciences, Hatfield, PA). Sections were analyzed by multispectral fluorescence microscopy using Pannoramic 250 1.14 slide scanner and Pannoramic Viewer 1.15 (3D Histech, Budapest, Hungary).

Statistical analysis

All data values are represented as mean ± standard error of the mean (SEM). Statistical analysis was performed using JMP8 software (SAS, Cary, NC). Two-sided pairwise t-test was applied for analysis. P-values < 0.05 were considered as statistically significant.

Results

Imaging of apoptosis in brain tumors

We have recently shown that anti-DR5 treatment led to significant apoptosis induction in subcutaneous D54-Caspase-3/7-GloSenor tumors (28). However, the more critical point to address is the potential of anti-DR5 antibody to induce apoptosis in orthotopic brain tumors. Bioluminescence imaging of untreated mice directly and 7 days after intracranial inoculation revealed weak but detectable basal bioluminescent signals which increased over time (Supplementary Fig. S1A). All animals showed quantifiable signals 7 days after inoculation indicating that spontaneous apoptotic events are sensitively detectable through the cranium and that the inoculated tumor cells grow in the brain parenchyma. The signal detection before treatment allowed the randomization of animals based on their basal apoptosis reporter signal and the expression of fold apoptosis induction after treatment.

Tumor cell spreading into spinal cord was observed by bioluminescence imaging in 19% of mice (Supplementary Fig. S1B). Histological analysis of explanted brains of affected mice revealed that tumor cells grew invasively into the lateral ventricle and distributed via the CSF into the spinal cord (Supplementary Fig. S1C). Mice with high signals in the spinal cord were excluded from study.

Determination of i.c. dosage response curve

To ensure optimal drug delivery by circumventing the BBB, anti-DR5-Cy5 was applied i.c. through the cranial burr hole into the same depth the cells were inoculated. Four different dosages were given i.c. to investigate dosage-dependent responses on apoptosis induction. Even the lowest dosage (0.005 mg/kg) led to a 4.5-fold apoptosis induction within 4 to 8 hours after application. The apoptosis induction steadily increased but less prominent between 0.05 and 0.2 mg/kg indicating saturation with anti-DR5-Cy5 (Fig. 2A and B). The fitted dosage response curve for i.c. application in Figure 2A allowed the quantification of the amount of antibody delivered to the tumor. Assuming a 100% drug delivery by i.c. application, the rate of apoptosis induction after systemic application of anti-DR5-Cy5 directly correlates with the amount of antibody which has reached the brain tumor. An almost 100% drug delivery for 0.005 and 0.02 mg/kg i.c. dosages was confirmed by 3DISCO and 2D immunofluorescence which visualized strong anti-DR5-Cy5 accumulation

in the brain tumor but low unspecific spreading in healthy brain tissue (Fig. 2C left and middle). At i.c. application of 0.05 and 0.2 mg/kg, however, DR5 receptors in the tumor tissue seem to be saturated and increasing amounts of anti-DR5-Cy5 were detected outside the tumor site. The dimensions of brain tumors could easily be determined due to bright lectin-A750 staining of chaotic tumor vessels but less prominent staining of healthy brain vessels (most likely due to resolution limitations of healthy brain capillaries smaller than 5 μm in diameter). H&E staining in consecutive sections confirmed localization of brain tumors in highly vascularized areas with prominent lectin-A750 staining (Fig. 2C right).

Determination of anti-DR5-Cy5 delivery over the BBB after i.v. application

The more clinical relevant application is the i.v. application. Therefore, we quantified the amount of antibody which was delivered to the brain tumor after i.v. injection by comparing the rate of apoptosis induction after i.c. and i.v. application. Monitoring anti-DR5-Cy5 accumulation in the brain tumor by *in vivo* fluorescence imaging could not been applied due to tremendous background noises in the whole body caused by circulating and unspecific accumulated anti-DR5-Cy5 even 24 hours after i.v. application (Supplement Fig. S2). Bioluminescence apoptosis imaging, however, allowed to sensitively detect the dosage-dependent effect on apoptosis induction when anti-DR5-Cy5 is given i.v. at different dosages. This indicates that the antibody has at least partially crossed the BBB and has targeted the tumor site. An i.v. dosage of 3 mg/kg led to a 20.8-fold increase. This dosage induces apoptosis slightly more than a 0.02 mg/kg dosage given i.c. (17.9-fold). An approximation of the delivered dose can be made by fitting a dosage response curve and using the resulting equation. Consequently, a 20.8-fold apoptosis induction after i.v. application of 3 mg/kg anti-DR5-Cy5 correlates with a 0.029 mg/kg i.c. given dosage (Fig. 3A and B). Assuming a 100% drug delivery after i.c. application, 0.97% of i.v. given antibody has passed the BBB and has reached the brain tumor. The 1 mg/kg i.v. given dosage led to a 2.8-fold apoptosis induction which equals to a 0.002 mg/kg i.c. dosage and, therefore, to a 0.20% drug delivery (Fig. 3A and B). For comparison, a quantitative assessment of i.v. and intratumoral (i.t.) anti-DR5-Cy5 application in a s.c. D54-Caspase-3/7 GloSensor model revealed that 3.90 to 7.00% of i.v. given anti-DR5-Cy5 reaches the tumor site (Supplementary Fig. S3).

Ex vivo quantification of anti-DR5-Cy5 fluorescent signals in the brain tumor region of i.v. and i.c. treated mice using 3DISCO confirmed the *in vivo* data (Fig. 3C and D left). I.c. application showed dosage-dependent increases in fluorescent signal intensities of accumulated anti-DR5-Cy5, which allows a determination of a dosage response curve according to dose-specific fluorescent signal intensities (Fig. 3C). Fluorescent signals after i.v. application of 1 mg/kg or 3 mg/kg anti-DR5-Cy5, respectively, revealed intensities comparable to 0.003 mg/kg or 0.028 mg/kg given i.c. which corresponds to 0.30% or 0.93% delivered anti-DR5-Cy5 (Fig. 3C). These calculated values are in good concordance with values defined by apoptosis reporter induction (0.20% or 0.97%) indicating a strong relationship between anti-DR5-Cy5 binding to and apoptosis induction in tumor cells (Fig. 3E). This relationship was further substantiated by immunohistochemistry. Sites of increased antibody binding to tumor cells showed intensified active caspase-3 staining (Fig.

3D right). Therefore, the pharmacodynamic read-out “apoptosis induction” can be used to make correct statements about the pharmacokinetic properties of anti-DR5-Cy5.

Efficacy study and monitoring apoptosis and tumor retention kinetics over time

After quantification of the amount of anti-DR5-Cy5 delivered to the brain tumor, we applied non-invasive imaging for monitoring apoptosis induction in an efficacy study. Apoptosis monitoring revealed that highest apoptosis induction was already observed 4 hours after application. Thereafter, apoptotic effects rapidly declined and were absent after 24 hours (Fig. 4A). Re-dosing of anti-DR5-Cy5 6 and 13 days (144 h and 312 h) after first treatment led to less severe apoptosis induction compared to first treatment and this effect lasted only for a few hours (Fig. 4A). After three i.v. applications of 3 mg/kg unspecific IgG or 1 mg/kg or 3 mg/kg anti-DR5-Cy5, endpoint volumes of brain tumors were determined by *ex vivo* 3DISCO. The dimensions of chaotic vessel structure defining the brain tumor demonstrated invasive tumor growth into lateral ventricle, corpus callosum and to the contralateral brain hemisphere in control mice and partly in low dosage treated mice (Fig. 4B and C). However, invasive brain tumor growth and tumor volume was significantly reduced in mice treated with 3 mg/kg anti-DR5-Cy5 ($p<0.05$) (Fig. 4B and C).

To explain the rapid decline of apoptosis induction in brain tumors, tumor retention kinetics of the antibody (3 mg/kg i.v.) were investigated in a follow-up study by sacrificing animals at different time points (4, 8, 12, 24 and 72 hours) and quantifying antibody accumulation in explanted brains. The fluorescence signal intensities in the brain tumors peaked after 4 hours (C_{max}) and dropped thereafter (Fig. 4D). Fifty percent of C_{max} was observed 19.3 hours after application and only 22.9% of C_{max} was retained after 72 hours. These kinetic data correlate with the pharmacodynamics graph of apoptosis induction (C_{max} after 4 hours, 50% of C_{max} after 12.5 hours, and 16.4% of C_{max} after 72 hours). In contrast, anti-DR5-Cy5 is longer retained in s.c. tumors. C_{max} of accumulated fluorescence signal intensity is only reached after 24 hours and 50% of C_{max} is still retained after 60.1 hours (Fig. 4E). This is in good concordance with pharmacodynamics data in s.c. tumor (50% of C_{max} after 65.9 hours).

Visualization of BBB impairment by penetration studies

The enhanced lectin staining in the neovasculature of the brain tumor and the slightly increased delivery of anti-DR5-Cy5 over the BBB (expected 0.1% for intact BBB, measured 0.20 to 0.97%) indicates modified vessel and BBB integrities in the brain tumor in contrast to healthy brain vessels. To assess modified penetration of large molecules from vessels to tumor tissue, lectin-A647 and human IgG-A750 antibody were applied i.v. 8 hours before sacrifice of mice. Fluorescent signals of lectin-A647 and IgG-A750 in overlayed 3DISCO scans of brain and s.c. tumor were quantified and plotted according to their distinct distances to vessel (Fig. 5A). The comparison of antibody penetration into the tissue from healthy brain vessels or brain tumor vessels, respectively, showed significant differences. While IgG-A750 penetrated more than 25 μm from brain tumor vessels into brain tumor tissue (AUC = 444.3), no quantifiable penetration from IgG-A750 out of healthy brain vessels was detected more than 15 μm from vessels (AUC = 61.8) (Fig. 5A, B and C). In contrast, approximately 2 to 4-fold higher amounts of IgG-A750 could penetrate several hundred

micrometers from tumor vessels without BBB into a s.c. tumor (AUC = 1368.0). Calculated from the AUCs, the BBB in the tumor area is partially disrupted on an average of 29.3% by the brain tumor [AUC (healthy) ≙ 0%; AUC (s.c. tumor) ≙ 100%] (Fig. 5B). U251 and U87-luc intracranial xenograft models showed even more BBB disruption (Supplementary Fig. S4).

Discussion

Here, we successfully applied non-invasive apoptosis imaging for quantifying the amount of antibody delivery to brain tumors and for monitoring the induction of apoptosis over time. By comparing apoptosis induction after i.v. with i.c. anti-DR5 application at different dosages, we determined the amount of anti-DR5 that has passed the partially disrupted BBB and has reached the brain tumor after systemic application. We found that 0.20 to 0.97% of the applied dosage had crossed the impaired BBB and these results correlate with previously determined values. Using a radioactivity-based pharmacokinetic model in different knockout mouse strains, Abuqayys et al found that 0.54 to 0.92% murine monoclonal IgG1 antibody passed the intact BBB (35). Banks et al showed that 0.11% of ^{131}I- or ^{125}I-labeled anti-amyloid beta antibody crosses an intact BBB in a mouse model of Alzheimer's disease (36). In breast cancer patients carrying brain metastases with intact BBB, trastuzumab, a humanized antibody against Her2, showed approximately 420 times lower concentrations in the CSF after systemic application in contrast to concentrations in the systemic circulation (~0.24% of trastuzumab in CSF) (37). In contrast, trastuzumab accumulated significantly higher in CSF when BBB was compromised either by prior radiotherapy (blood-to-CSF ratio of 76:1) or in patients with concurrent meningeal carcinomatosis (ratio 49:1) (37). In these cases of BBB impairment, up to 2% of trastuzumab could enter the CSF. The GBM cell line D54-MG is known to grow invasive and to migrate along blood vessels which might impair the BBB (38). Moreover, these tumor cells might disrupt the BBB through cytokine release (39). A complete disruption of the BBB in D54-MG xenografts as indicated by Blasberg et al, however, could not been confirmed (40). Blasberg et al found that levels of i.v. applied antibodies in D54-MG brain tumors are in the same range as in s.c. tumors. In contrast to these results, we determined less than 1% of anti-DR5-Cy5 reaching the brain tumor whereas up to 7% has reached a s.c. tumor indicating the presence of an at least partially functional BBB (see Fig. 3 and Supplementary Fig. S3). Concordantly, Sarin et al found by dynamic contrast-enhanced MRI that gadolinium-labeled dendrimers penetrated more into ectopic intramuscular RG-2 tumors than in RG-2 orthotopic brain tumors (41). A partial impairment of 29.3% of the BBB by tumor growth, however, was detected by antibody penetration studies (Fig. 5) which explains the slightly increased antibody delivery to the brain tumor. This finding is substantiated by Qin et al who determined by ^{99M}Tc-GH emission computed tomography that 22.1% of the BBB is destroyed only by the brain tumor growth. Radiotherapy further increases BBB disruption to an average of 74.7% in brain tumor patients (42).

Despite the fact that less than 1% of anti-DR5-Cy5 reaches the brain tumor, the delivered dosage to the tumor is sufficient to deploy significant anti-tumor efficacy when anti-DR5-Cy5 is applied i.v. in adequately high dosages (3 mg/kg or more). Since the BBB is impaired in most high grade gliomas as well as in our investigated intracranial xenograft models

(D54, U251, U87), the BBB crossing of antibody might not be the limiting factor and the main reason for the lack of efficacy in the clinical situation (43). In fact, mutation in or activation of multiple aberrant signaling pathways resulting in resistance to monotherapy, the migration of tumor cells from the necrotic tumor core along blood vessels with completely intact and impenetrable BBB or poor retention times of therapeutics in the brain would limit the efficacy of anti-tumor compounds in highly heterogeneous brain tumors (13, 44–47).

For the first time, we were able to monitor the pharmacodynamics of an antibody by quantifying apoptosis in brain tumors non-invasively over time. Monitoring revealed that initial apoptosis induction rapidly declined after 8 hours and was absent after 24 hours which correlates with antibody retention times in the brain tumors (Fig. 4A and D). In contrast, anti-DR5 showed long lasting apoptosis induction over days in the related s.c. xenograft model (Fig. 4E) (28). Concordantly, Burvenich et al determined prolonged tumor retention of an anti-DR5 antibody and associated anti-tumor efficacy in s.c. colon cancer models by radioactivity-based biodistribution studies and CT imaging (48). The short apoptosis induction and antibody retention specifically in brain tumors can be explained by a fast clearance of anti-DR5 via rapid turnover of cerebral fluids or receptor-mediated efflux of antibodies out of the brain (35, 49). These results provide novel insights into the pharmacokinetics of antibodies in brain tumors substantiating it as reason for the failure of therapeutical antibodies to efficiently treat high grade brain tumors. The main limitation of our approach consists in the fact that it is only applicable for apoptosis-inducing compounds. Primarily non-apoptotic compounds such as cetuximab or erlotinib did not activate the apoptosis reporter in reasonable amounts (data not shown). Moreover, the dosage response curve has to be determined for each drug assessment by i.c. application of the drug in at least four different dosages. Higher i.c. dosages did not show 100% drug delivery because anti-DR5-Cy5 was also detected unspecifically distributed around the brain tumor (Fig. 2). This might be due to a saturation effect of DR5 with anti-DR5-Cy5 on tumor cells. Consequently, the dosage response curve flattens above i.c. dosages of 0.02 mg/kg anti-DR5-Cy5 so that only a limited i.v. dosage range can be evaluated. Larger brain tumors, however, might show saturation at higher dosages so that initiation of drug application at later time-points (>8 days after cell inoculation) might solve this limitation. Therefore, a study starting with larger brain tumors (>1 mm^3) should be conducted to investigate the anti-tumor effect of anti-DR5 on established brain tumors. Ultimately, the apoptosis reporter technology cannot be transferred to clinical investigations because the tumor cells need to be stably transfected with the reporter construct.

Nevertheless, this technology allows quantification of BBB crossing of pro-apoptotic compounds in preclinical models without expensive PET/SPECT-imagers and the use of radioactivity or labor-intensive cranial window technique. Moreover, monitoring apoptosis in brain tumors over time provides a feasible, reliable and urgently needed pharmacodynamic readout to investigate the activity of systemically applied compounds in brain tumors relative to their dosage in detail (4). Thus, dosage, scheduling and combination therapies of pro-apoptotic drugs and radiotherapy can be optimized in preclinical models of brain tumors and provide rationales to improve clinical study designs. Particularly, the simultaneous assessment of pharmacodynamic and –kinetic properties of modified

antibodies, aiming to enhance penetration across the partially functional BBB, can be facilitated and evaluated for clinical application (50).

The technology described herein demonstrates that 0.20 to 0.97% of systemically applied anti-DR5-Cy5 has reached the brain tumor in an intracranial GBM xenograft model with 29.3% impaired BBB. The delivered amount of anti-DR5-Cy5 strongly induced apoptosis 4 to 8 hours after application but experienced rapid decline in apoptotic activity and tumor retention thereafter; most likely due to a fast clearance of anti-DR5-Cy5 out of the brain. Systemic treatment of brain tumors with adequate anti-DR5-Cy5 dosages (3 mg/kg or more) showed significant anti-tumor efficacy due to strong initial apoptosis induction.

Supplementary Material

Refer to Web version on PubMed Central for supplementary material.

Acknowledgments

The authors would like to thank Julia Mathejczyk for constructive discussions. T.G. Weber would like to thank Michael Stürzl for supervising his Ph.D. thesis. A. Rehemtulla and S. Galbán were supported by the National Institutes of Health (P01CA085878).

Financial support: TGW, FO, AR, TP, WS: Roche Diagnostics GmbH; SG, AR: National Institutes of Health (P01CA085878).

References

1. Frank RT, Aboody KS, Najbauer J. Strategies for enhancing antibody delivery to the brain. Biochim Biophys Acta. 2011; 1816:191–8. [PubMed: 21767610]
2. Grossi PM, Ochiai H, Archer GE, McLendon RE, Zalutsky MR, Friedman AH, et al. Efficacy of intracerebral microinfusion of trastuzumab in an athymic rat model of intracerebral metastatic breast cancer. Clin Cancer Res. 2003; 9:5514–20. [PubMed: 14654531]
3. Chamberlain MC. Anticancer therapies and CNS relapse: overcoming blood-brain and blood-cerebrospinal fluid barrier impermeability. Expert Rev Neurother. 2010; 10:547–61. [PubMed: 20367207]
4. Watts RJ, Dennis MS. Bispecific antibodies for delivery into the brain. Curr Opin Chem Biol. 2013; 17:393–9. [PubMed: 23570979]
5. Siegal T. Which drug or drug delivery system can change clinical practice for brain tumor therapy? Neuro Oncol. 2013; 15:656–69. [PubMed: 23502426]
6. Meikle SR, Matthews JC, Brock CS, Wells P, Harte RJ, Cunningham VJ, et al. Pharmacokinetic assessment of novel anti-cancer drugs using spectral analysis and positron emission tomography: a feasibility study. Cancer Chemother Pharmacol. 1998; 42:183–93. [PubMed: 9685053]
7. Marzolini C, Decosterd LA, Shen F, Gander M, Leyvraz S, Bauer J, et al. Pharmacokinetics of temozolomide in association with fotemustine in malignant melanoma and malignant glioma patients: comparison of oral, intravenous, and hepatic intra-arterial administration. Cancer Chemother Pharmacol. 1998; 42:433–40. [PubMed: 9788568]
8. Ostermann S, Csajka C, Buclin T, Leyvraz S, Lejeune F, Decosterd LA, et al. Plasma and cerebrospinal fluid population pharmacokinetics of temozolomide in malignant glioma patients. Clin Cancer Res. 2004; 10:3728–36. [PubMed: 15173079]
9. Johnson DR, O'Neill BP. Glioblastoma survival in the United States before and during the temozolomide era. J Neurooncol. 2012; 107:359–64. [PubMed: 22045118]
10. Fukai J, Nishio K, Itakura T, Koizumi F. Antitumor activity of cetuximab against malignant glioma cells overexpressing EGFR deletion mutant variant III. Cancer Sci. 2008; 99:2062–9. [PubMed: 19016767]

11. Mineo JF, Bordron A, Quintin-Roué I, Loisel S, Ster KL, Buhé V, et al. Recombinant humanised anti-HER2/neu antibody (Herceptin®) induces cellular death of glioblastomas. Br J Cancer. 2004; 91:1195–9. [PubMed: 15328518]
12. Bagci-Onder T, Agarwal A, Flusberg D, Wanningen S, Sorger P, Shah K. Real-time imaging of the dynamics of death receptors and therapeutics that overcome TRAIL resistance in tumors. Oncogene. 2012; 32:2818–27. [PubMed: 22824792]
13. Wong MLH, Kaye AH, Hovens CM. Targeting malignant glioma survival signalling to improve clinical outcomes. J Clin Neurosci. 2007; 14:301–8. [PubMed: 17276069]
14. Neyns B, Sadones J, Joosens E, Bouttens F, Verbeke L, Baurain JF, et al. Stratified phase II trial of cetuximab in patients with recurrent high-grade glioma. Ann Oncol. 2009; 20:1596–603. [PubMed: 19491283]
15. Lin NU, Bellon JR, Winer EP. CNS metastases in breast cancer. J Clin Oncol. 2004; 22:3608–17. [PubMed: 15337811]
16. Rich JN, Bigner DD. Development of novel targeted therapies in the treatment of malignant glioma. Nat Rev Drug Discov. 2004; 3:430–46. [PubMed: 15136790]
17. Aprile I, Muti M, Principi M, Bartolini N, Zenoni A, Tazza G, et al. A Magnetic Resonance comparative study between enhancement, rCBV and ACD in brain glioblastomas. Radiol Med. 2002; 104:87–91. [PubMed: 12386559]
18. Schlageter KE, Molnar P, Lapin GD, Groothuis DR. Microvessel organization and structure in experimental brain tumors: microvessel populations with distinctive structural and functional properties. Microvasc Res. 1999; 58:312–28. [PubMed: 10527772]
19. Rubenstein JL, Fridlyand J, Abrey L, Shen A, Karch J, Wang E, et al. Phase I study of intraventricular administration of rituximab in patients with recurrent CNS and intraocular lymphoma. J Clin Oncol. 2007; 25:1350–6. [PubMed: 17312328]
20. Daghighian F, Pentlow KS, Larson SM, Graham MC, DiResta GR, Yeh SD, et al. Development of a method to measure kinetics of radiolabelled monoclonal antibody in human tumour with applications to microdosimetry: positron emission tomography studies of iodine-124 labelled 3F8 monoclonal antibody in glioma. Eur J Nucl Med. 1993; 20:402–9. [PubMed: 8519259]
21. Holdhoff M, Supko JG, Gallia GL, Hann CL, Bonekamp D, Ye X, et al. Intratumoral concentrations of imatinib after oral administration in patients with glioblastoma multiforme. J Neurooncol. 2010; 97:241–5. [PubMed: 19768386]
22. Friden PM, Walus LR, Musso GF, Taylor MA, Malfroy B, Starzyk RM. Anti-transferrin receptor antibody and antibody-drug conjugates cross the blood-brain barrier. Proc Natl Acad Sci U S A. 1991; 88:4771–5. [PubMed: 2052557]
23. Neuwelt EA, Barnett PA, Hellström KE, Hellström I, McCormick CI, Ramsey FL. Effect of blood-brain barrier disruption on intact and fragmented monoclonal antibody localization in intracerebral lung carcinoma xenografts. J Nucl Med. 1994; 35:1831–41. [PubMed: 7965166]
24. Iqbal U, Trojahn U, Albaghdadi H, Zhang J, O'Connor-McCourt M, Stanimirovic D, et al. Kinetic analysis of novel mono- and multivalent VHH-fragments and their application for molecular imaging of brain tumours. Br J Pharmacol. 2010; 160:1016–28. [PubMed: 20590596]
25. Vajkoczy P, Ullrich A, Menger MD. Intravital fluorescence videomicroscopy to study tumor angiogenesis and microcirculation. Neoplasia. 2000; 2:53–61. [PubMed: 10933068]
26. Yuan F, Salehi HA, Boucher Y, Vasthare US, Tuma RF, Jain RK. Vascular permeability and microcirculation of gliomas and mammary carcinomas transplanted in rat and mouse cranial windows. Cancer Res. 1994; 54:4564–8. [PubMed: 8062241]
27. Galbán S, Jeon YH, Bowman BM, Stevenson J, Sebolt KA, Sharkey LM, et al. Imaging proteolytic activity in live cells and animal models. PloS one. 2013; 8:e66248. [PubMed: 23776643]
28. Weber TG, Pöschinger T, Galbán S, Rehemtulla A, Scheuer W. Noninvasive monitoring of pharmacodynamics and kinetics of a Death Receptor 5 antibody and its enhanced apoptosis induction in sequential application with doxorubicin. Neoplasia. 2013; 15:863–74. [PubMed: 23908588]
29. Fiveash JB, Gillespie GY, Oliver PG, Zhou T, Belenky ML, Buchsbaum DJ. Enhancement of glioma radiotherapy and chemotherapy response with targeted antibody therapy against death receptor 5. Int J Radiat Oncol Biol Phys. 2008; 71:507–16. [PubMed: 18474311]

30. Saito R, Bringas JR, Panner A, Tamas M, Pieper RO, Berger MS, et al. Convection-enhanced delivery of tumor necrosis factor-related apoptosis-inducing ligand with systemic administration of temozolomide prolongs survival in an intracranial glioblastoma xenograft model. Cancer Res. 2004; 64:6858–62. [PubMed: 15466173]
31. Nagane M, Pan G, Weddle JJ, Dixit VM, Cavenee WK, Huang HJ. Increased death receptor 5 expression by chemotherapeutic agents in human gliomas causes synergistic cytotoxicity with tumor necrosis factor-related apoptosis-inducing ligand in vitro and in vivo. Cancer Res. 2000; 60:847–53. [PubMed: 10706092]
32. Adams, C. DR5 antibodies and uses thereof. WIPO Patent. 2006083971. 2006.
33. Ertürk A, Becker K, Jährling N, Mauch CP, Hojer CD, Egen JG, et al. Three-dimensional imaging of solvent-cleared organs using 3DISCO. Nat Protoc. 2012; 7:1983–95. [PubMed: 23060243]
34. Dobosz M, Strobel S, Ntziachristos V, Scheuer W. Three-dimensional visualization of tumor vessel architecture and antibody penetration using multispectral fluorescence ultramicroscopy. WMIC Dublin. 2012; P323
35. Abuqayyas L, Balthasar JP. Investigation of the role of FcγR and FcRn in mAb distribution to the brain. Mol Pharm. 2013; 10:1505–13. [PubMed: 22838637]
36. Banks WA, Terrell B, Farr SA, Robinson SM, Nonaka N, Morley JE. Passage of amyloid β protein antibody across the blood–brain barrier in a mouse model of Alzheimer's disease. Peptides. 2002; 23:2223–6. [PubMed: 12535702]
37. Stemmler HJ, Schmitt M, Willems A, Bernhard H, Harbeck N, Heinemann V. Ratio of trastuzumab levels in serum and cerebrospinal fluid is altered in HER2-positive breast cancer patients with brain metastases and impairment of blood-brain barrier. Anticancer Drugs. 2007; 18:23–8. [PubMed: 17159499]
38. Lyons SA, Chung WJ, Weaver AK, Ogunrinu T, Sontheimer H. Autocrine glutamate signaling promotes glioma cell invasion. Cancer Res. 2007; 67:9463–71. [PubMed: 17909056]
39. Criscuolo GR, Merrill MJ, Oldfield EH. Characterization of a protein product of human malignant glial tumors that induces microvascular permeability. Adv Neurol. 1990; 52:469–74. [PubMed: 2396540]
40. Blasberg RG, Nakagawa H, Bourdon MA, Groothuis DR, Patlak CS, Bigner DD. Regional localization of a glioma-associated antigen defined by monoclonal antibody 81C6 in vivo: kinetics and implications for diagnosis and therapy. Cancer Res. 1987; 47:4432–43. [PubMed: 3607773]
41. Sarin H, Kanevsky AS, Wu H, Sousa AA, Wilson CM, Aronova MA, et al. Physiologic upper limit of pore size in the blood-tumor barrier of malignant solid tumors. J Transl Med. 2009; 7:51. [PubMed: 19549317]
42. Qin DX, Zheng R, Tang J, Li JX, Hu YH. Influence of radiation on the blood-brain barrier and optimum time of chemotherapy. Int J Radiat Oncol Biol Phys. 1990; 19:1507–10. [PubMed: 2262373]
43. Tzeng SY, Green JJ. Therapeutic nanomedicine for brain cancer. Ther Deliv. 2013; 4:687–704. [PubMed: 23738667]
44. Wen PY, Schiff D, Cloughesy TF, Raizer JJ, Laterra J, Smitt M, et al. A phase II study evaluating the efficacy and safety of AMG 102 (rilotumumab) in patients with recurrent glioblastoma. Neuro Oncol. 2011; 13:437–46. [PubMed: 21297127]
45. Wilhelm I, Molnár J, Fazakas C, Haskó J, Krizbai IA. Role of the blood-brain barrier in the formation of brain metastases. Int J Mol Sci. 2013; 14:1383–411. [PubMed: 23344048]
46. Agarwal S, Manchanda P, Vogelbaum MA, Ohlfest JR, Elmquist WF. Function of the blood-brain barrier and restriction of drug delivery to invasive glioma cells: findings in an orthotopic rat xenograft model of glioma. Drug Metab Dispos. 2013; 41:33–9. [PubMed: 23014761]
47. Pels H, Schulz H, Schlegel U, Engert A. Treatment of CNS lymphoma with the anti-CD20 antibody rituximab: experience with two cases and review of the literature. Onkologie. 2003; 26:351–4. [PubMed: 12972702]
48. Burvenich IJ, Lee FT, Cartwright GA, O'Keefe GJ, Makris D, Cao D, et al. Molecular Imaging of Death Receptor 5 Occupancy and Saturation Kinetics In Vivo by Humanized Monoclonal Antibody CS-1008. Clin Cancer Res. 2013; 19:5984–93. [PubMed: 24045184]

49. Zhang Y, Pardridge WM. Mediated efflux of IgG molecules from brain to blood across the blood-brain barrier. J Neuroimmunol. 2001; 114:168–72. [PubMed: 11240028]

50. Pardridge WM. Re-engineering biopharmaceuticals for delivery to brain with molecular Trojan horses. Bioconjug Chem. 2008; 19:1327–38. [PubMed: 18547095]

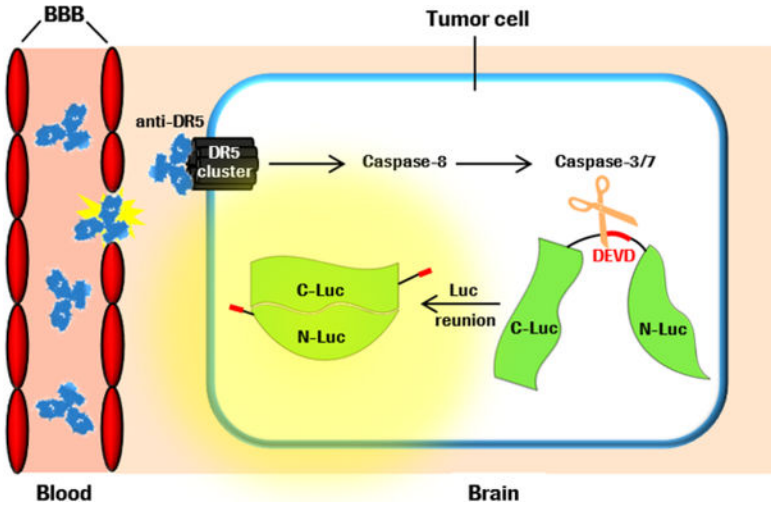

Figure 1.

Schematic illustration of anti-DR5 crossing an impaired BBB, Caspase-3/7 activation after anti-DR5 binding to Death Receptor 5 cluster, cleavage of constitutively expressed apoptosis reporter construct C-Luc-DEVD-N-Luc, complementation of C-Luc and N-Luc, and light emission after external addition of luciferin.

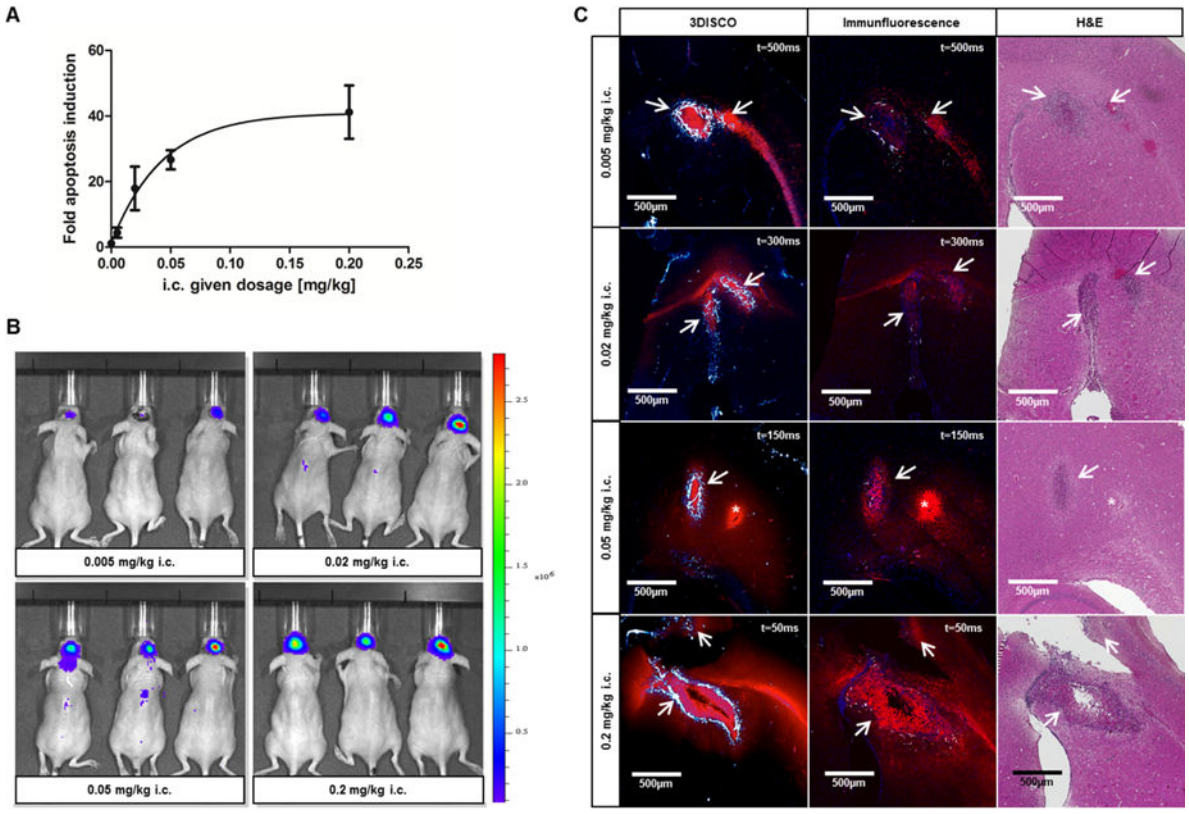

Figure 2.

Dosage response curve and evaluation of drug delivery after i.c. application. (A) Dosage response curve showing fold induction of apoptosis reporter activity after i.c. application of 0.005, 0.02, 0.05, and 0.2 mg/kg anti-DR5-Cy5. Curve was fitted by nonlinear regression. (B) Representative BLI images 4 hours after i.c. application of anti-DR5-Cy5 at different dosages. (C) Representative 3DISCO (left) and related immunofluorescence (middle) and H&E (right) images showing anti-DR5-Cy5 distribution (red) in the brain after i.c. application. Strong lectin vessel staining (white-blue) in 3DISCO images allows localization of brain tumor site (arrows); t = exposure time; * Injection channel, middle panel: Cell nuclei (blue).

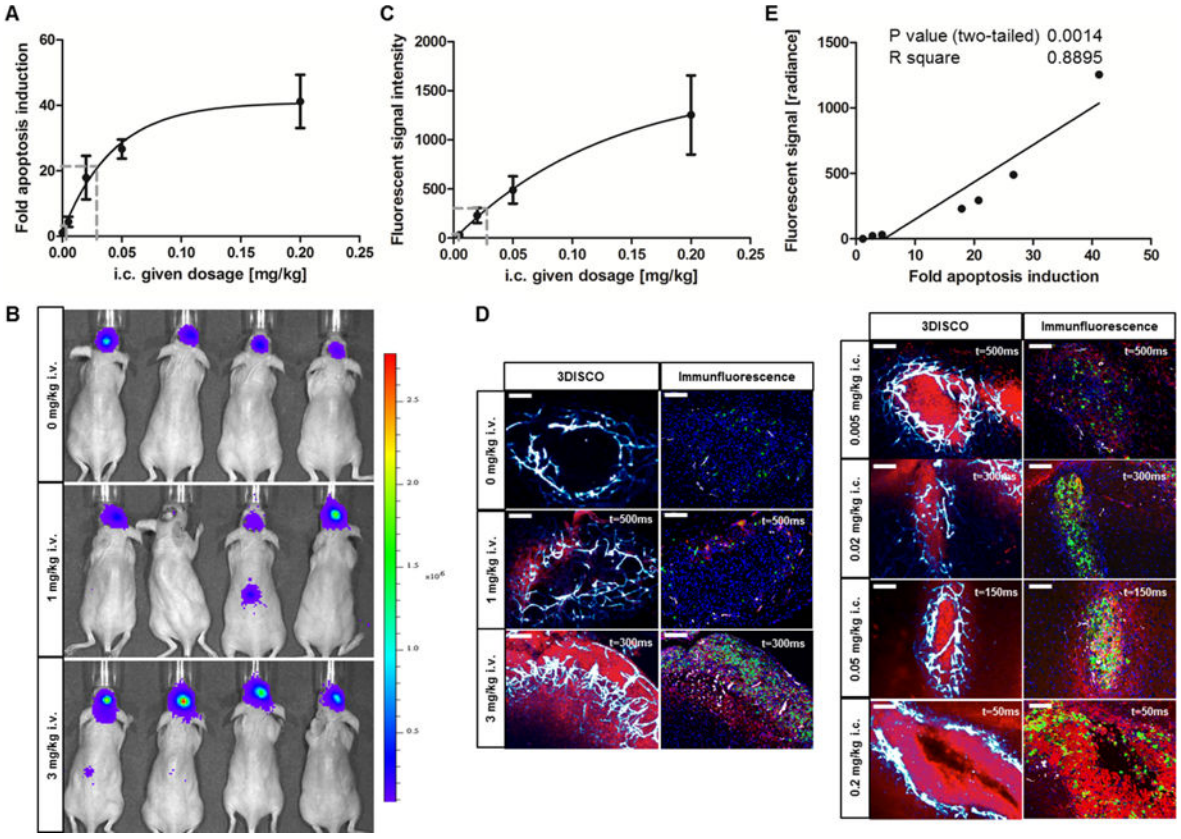

Figure 3.

Apoptosis induction and anti-DR5-Cy5 accumulation in brain tumors. (A) Fold apoptosis induction after i.v. anti-DR5-Cy5 application (dashed lines) is ranged in the dosage response curve. (B) Representative BLI images 8 hours after i.v. application of control IgG (3 mg/kg) or anti-DR5-Cy5 (1 mg/kg or 3 mg/kg). (C) Dosage response curve of fluorescent signal intensities measured by 3DISCO in the brain tumors after i.c. anti-DR5-Cy5 application. Curve was fitted by nonlinear regression. Fold apoptosis induction after i.v. application and the related i.c. dosage are marked with dashed lines. (D) Representative 3DISCO (left row) and immunofluorescence (right row) images. Highly vascularized brain tumors (white-blue) showed dose and application-dependent accumulation of anti-DR5-Cy5 (red) and corresponding caspase-3 activation (green). Caspase-3 activation signal (green) was scanned with t = 50ms on each slide to compare images. Exposure times for Cy5 antibody fluorescent signals (red) are denoted; original magnification 400×; scale bars: 100 μm. (E) Correlation analysis of fluorescent signals and apoptosis induction in brain tumors after anti-DR5-Cy5 treatment in different dosages and applications. Plotted values represent means of 0.005, 0.02, 0.05, and 0.2 mg/kg i.c. and 0, 1, and 3 mg/kg i.v. anti-DR5-Cy5 treated mice.

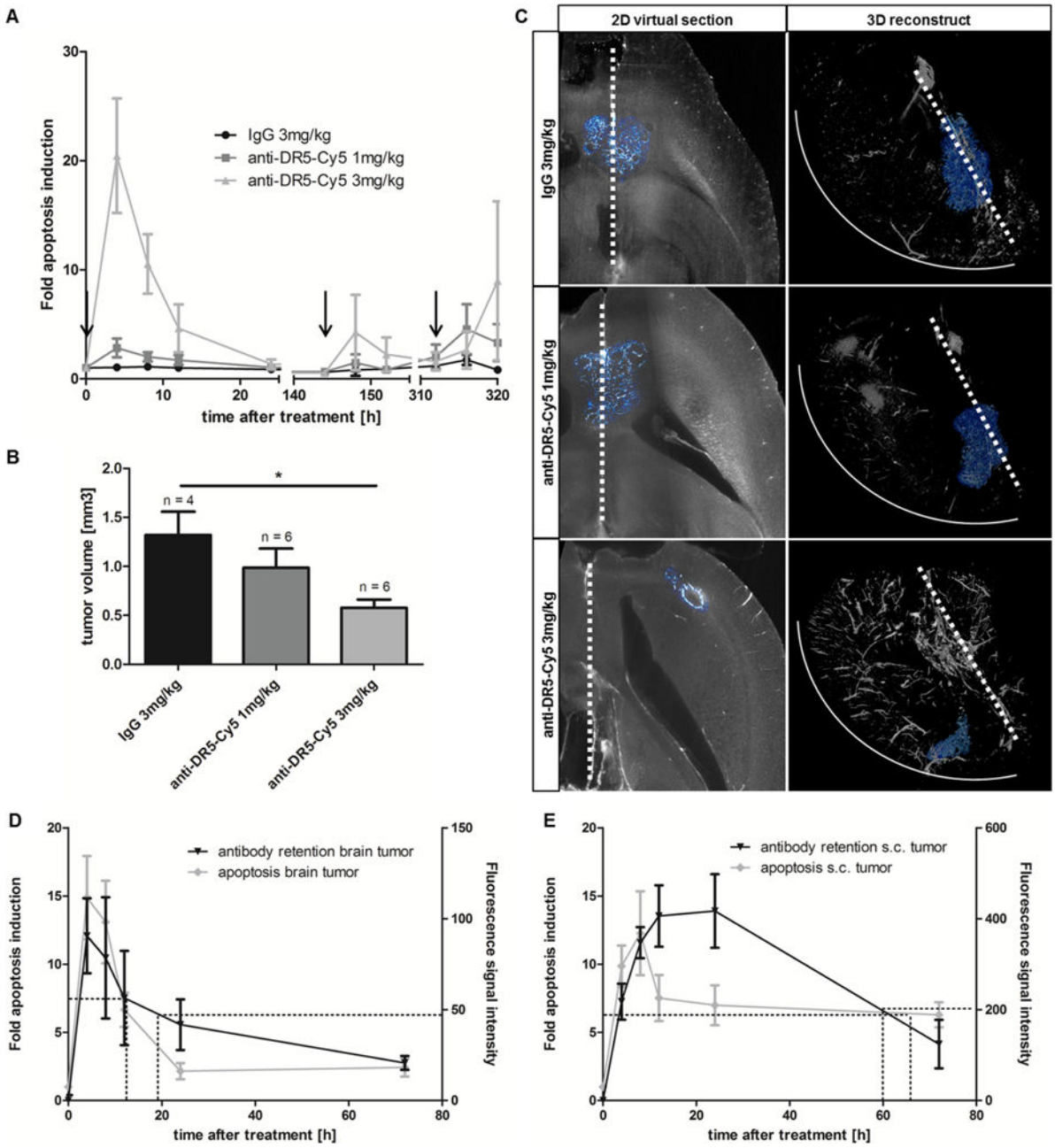

Figure 4.

Pharmacodynamics, tumor retention kinetics and efficacy after anti-DR5-Cy5 treatment. (A) Pharmacodynamic time course of apoptosis induction during therapy. Arrows indicate drug application. (B) Tumor volumes at endpoint of efficacy study. Tumor volumes were determined by 3DISCO of stained tumor vessels in explanted brains; *$p < 0.05$. (C) Representative 2D virtual sections and related 3-dimensional reconstructed brains showing the location, invasive growth and volume of brain tumors (white-blue) at endpoint of efficacy study. Dimensions of brain tumors were determined by lectin staining. Dashed line: corpus callosum/midline of brain; solid line: outer rim of right brain hemisphere. (D) Apoptosis induction dynamics and tumor retention kinetics of anti-DR5-Cy5 (3 mg/kg i.v.)

over 72 hours in brain tumors. 50% decline is marked by dashed lines; n = 5. (E) Apoptosis induction dynamics and tumor retention kinetics of anti-DR5-Cy5 (3 mg/kg i.v.) over 72 hours in s.c. tumors. 50% decline is marked by dashed lines; n = 5.

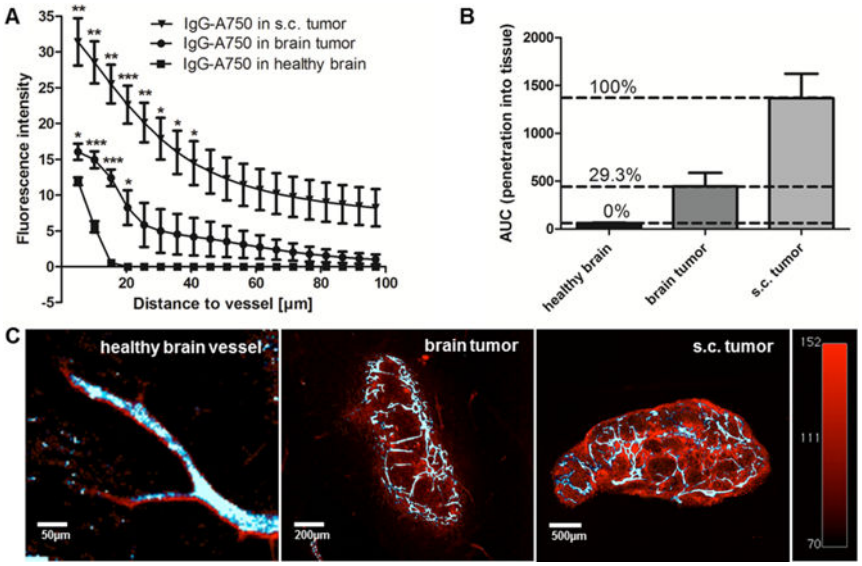

Figure 5.

Different penetration of i.v. applied, unspecific IgG-A750 out of healthy, s.c. or brain tumor vessels. (A) Graphs displaying mean IgG-A750 fluorescent signals as a function of distance from the nearest healthy brain or tumor vessel; *p < 0.05, **p < 0.02, ***p < 0.01; n = 4. (B) AUCs of penetration graphs displayed in (A) and the related percentage of BBB disruption. (C) Representative 3DISCO overlay images of lectin-A647 staining (white-blue) and IgG-A750 distribution (red) to depict IgG-A750 penetration into surrounding tissue. Color scales and exposure times of different samples were standardized to compare images.